A&A 486, 941–950 (2008)
DOI: 10.1051/0004-6361:200809405

Astronomy & Astrophysics

Abundance variations in the globular cluster M71 (NGC 6838)⋆

A. Alves-Brito[1], R. P. Schiavon[2], B. Castilho[3], and B. Barbuy[1]

[1] Universidade de São Paulo, IAG, Rua do Matão 1226, Cidade Universitária, São Paulo 05508-900, Brazil
e-mail: [abrito;barbuy]@astro.iag.usp.br
[2] Department of Astronomy, University of Virginia, PO Box 3818, Charlottesville, VA 22903-0818, USA
e-mail: rps7v@mail.astro.virginia.edu
[3] Laboratório Nacional de Astrofísica/MCT, CP 21, Itajubá, MG, 37500-000, Brazil
e-mail: bruno@lna.br

Received 16 January 2008 / Accepted 22 April 2008

ABSTRACT

Context. Abundance variations in moderately metal-rich globular clusters can give clues about the formation and chemical enrichment of globular clusters.
Aims. CN, CH, Na, Mg and Al indices in spectra of 89 stars of the template metal-rich globular cluster M71 are measured and implications on internal mixing are discussed.
Methods. Stars from the turn-off up to the Red Giant Branch ($0.87 < \log g < 4.65$) observed with the GMOS multi-object spectrograph at the Gemini-North telescope are analyzed. Radial velocities, colours, effective temperatures, gravities and spectral indices are determined for the sample.
Results. Previous findings related to the CN bimodality and CN-CH anticorrelation in stars of M71 are confirmed. We also find a CN-Na correlation, and Al-Na, as well as an Mg_2-Al anticorrelation.
Conclusions. A combination of convective mixing and a primordial pollution by AGB or massive stars in the early stages of globular cluster formation is required to explain the observations.

Key words. globular clusters: individual: M71 – stars: abundances – stars: atmospheres – Galaxy: abundances

1. Introduction

Globular Clusters (GCs) provide important information on the early chemical and dynamical evolution of the Milky Way.

Star-to-star abundance variations of light elements – Li, C, N, O, Na, Mg, and Al – are extensively reported in the literature (Gratton et al. 2004, and references therein). Li variations among turnoff (TO) stars and a Li-Na anticorrelation have been reported; among giant stars, C and N abundances, as well as the pairs O:Na and Al:Mg are also found to be anticorrelated. Such anomalies have not been obtained for heavier elements. These abundance variations have been reported in the literature over the past two decades, but their origin is still widely debated.

Some of the abundance variations seen in globular-cluster giants can be explained by evolutionary mixing with migration of processed material through the CNO cycle to the surface of giant stars (Iben 1964; Charbonnel 1994), whereas a primordial-enrichment scenario, which requires early contamination of intracluster material, is claimed by some authors (e.g. Smith 1987; Kraft 1994).

With a moderately high metallicity ($\langle$[Fe/H]$\rangle = -0.73$, Harris 1996), and an old age of 10−12 Gyr (Grundahl et al. 2002; Meissner & Weiss 2006), M71 is often regarded as a prototype of northern metal-rich globular clusters and considered as a suitable globular cluster to study abundance variations. It is located near the Galactic plane ($b = -4.6°$) and has a reddening of $E(B-V) = 0.27 \pm 0.05$ and an apparent distance modulus of $(m-M)_V = 13.60 \pm 0.10$ (Geffert & Maintz 2000). Dinescu et al. (1999) have obtained space velocities for a set of Galactic globular clusters. For M71 they determined velocity components $(U, V, W) = (77 \pm 14, -58 \pm 10, -2 \pm 14)$ km s^{-1} and a low eccentricity orbit, which characterizes M71, kinematically, as a thick-disk cluster.

Chemical abundances were discussed in several previous studies of this cluster, including DDO photometry of giant stars (Hesser et al. 1977; Briley et al. 2001) and low- and high-resolution analysis of stars in different evolutionary stages from the Main-Sequence (MS) TO to the Red Giant Branch (RGB) tip (Cohen 1980; Smith & Norris 1982; Leep et al. 1987; Smith & Penny 1989; Penny et al. 1992; Sneden et al. 1994; Cohen 1999; Ramirez & Cohen 2002; Lee et al. 2004; Lee 2005; Boesgaard et al. 2005; Yong et al. 2006). Many of these studies show a CN bimodality, with CN-CH anticorrelation, Na-O anticorrelation and variations in Al abundance.

In this paper we present the main results of an analysis of high S/N, medium resolution, Gemini/GMOS spectra of a large number of M71 stars, from the main-sequence turnoff to the tip of the giant branch. Our goals are twofold: to improve the statistics on abundance variations in M71 stars; and to study the behaviour of 14 spectral indices for the sample stars in order to shed light on the main astrophysical processes leading to the observed star-to-star abundance variations. We estimate the C

⋆ Tables 1, 3−5 are only available in electronic form at the CDS via anonymous ftp to cdsarc.u-strasbg.fr (130.79.128.5) or via http://cdsweb.u-strasbg.fr/cgi-bin/qcat?J/A+A/486/941

and N abundances of one CN-strong and one CN-weak giant from spectrum synthesis, based on state-of-the-art model photospheres and an up-to-date line list. A comparison of our results with those based on recent high-resolution abundance analysis is also presented.

This paper is structured as follows. The observations and data reductions are described in Sect. 2. The analysis of radial velocities, photometry, atmospheric parameters and line indices is presented in Sect. 3. In Sect. 4 the results are shown, and in Sect. 5 they are discussed and contrasted with previous studies. Our conclusions are summarized in Sect. 6.

2. Observations and data reduction

Imaging and spectroscopy of M71 stars were obtained with the Gemini Multi-Object Spectrograph (GMOS; see, for example, Hook et al. 2004, for more details) in the MOS mode on the 8 m Frederick C. Gillett Telescope (Gemini-North).

On July 18, 2002, the pre-imaging required to build four GMOS masks was obtained. It superposes a GMOS-North field over 5.5 × 5.5 arcmin. The image of the M71 field was obtained using the *r_G0303* filter, with an effective wavelength of 6300 Å and wavelength coverage of 5620−6980 Å. Exposures of 4 × 180 s were taken, with the CCD detector operating at 4 electrons/DN and a readout noise of 6.6 electrons. The mean airmass during the pre-imaging observation was 1.157. Thus, using a finding-chart available in Cudworth (1985), 145 M71 stars were identified in the GMOS image and selected for spectroscopic observations.

Spectroscopic data were collected on August 5, 2002, using the B600+_G5303 (600 lines/mm) grating and adopting arcsec-wide slits. The CCDs were binned in a 2 × 2 mode (along both the spatial and dispersion axes). This configuration achieved a spectral resolution $R \sim 2000$ at 5100 Å with a dispersion of 0.0917 nm/pix, covering from 3500 to 7000 Å.

The 145 target stars were selected in order to give appropriate sampling of the colour magnitude diagram (CMD). The maximum time for each individual exposure was constrained by the bright red giants of the cluster. Short exposures were taken in order to avoid saturation and a number of these exposures for the faintest stars of the turn-off were co-added. The total integration time was defined by our desire to achieve $S/N \sim 150$ at $\lambda \sim 4000$ Å. Finally, spectra of the spectrophotometric standard star EG 131 were obtained using a 1-arcsec longslit, with the same instrumental set up as adopted for the science observations.

Science and standard star data were both reduced using the GEMINI GMOS Data Reduction Package within the IRAF package. Bias frames, flat-fields and CuAr images were taken as part of the GEMINI base calibrations. At this point, the reduction process comprised bias-subtraction and flat-fielding, using GCAL flats which were previously co-added and normalized. Cosmic rays were then cleaned. The wavelength calibration was carried out with solutions obtained from the CuAr arc exposures, which provided typical residuals of 0.2 Å. Spectra were then sky-subtracted and extracted into a series of 1D spectra. All spectra were extinction-corrected using the mean extinction coefficients obtained for Mauna Kea. As a result of the location of the *slits* with respect to the mask-bisector, the wavelength coverage varies from star to star. In addition, two gaps corresponding to 0.5 mm between CCDs are also present in the final spectra.

3. Analysis

3.1. Heliocentric radial velocities

Heliocentric radial velocities for the sample stars were obtained using both *rvidlines* and *fxcor* IRAF procedures. The former measures radial velocities from spectra by determining the wavelength shift in spectral lines relative to specified rest wavelengths and the measured velocities are corrected to a heliocentric frame of reference. We derived a mean heliocentric radial velocity of -12 ± 46 km s^{-1} ($N = 145$ stars). The task *fxcor*, on the other hand, performs a Fourier cross-correlation between lists of input object and template spectra. A set of 77 spectral templates with stellar parameters given by: [Fe/H] = −1.00, [α/Fe] = 0.00, $4250 \leq T_{\rm eff} \leq 5750$ K and $0.00 \leq \log g \leq 5.0$ dex were taken from the library of synthetic stellar spectra by Coelho et al. (2005). Measurements of 142 stars led to a mean heliocentric radial velocity of 11 ± 49 km s^{-1}.

The mean difference between the heliocentric radial velocities as measured in two ways ($v^{\rm h}_{\rm fxcor} - v^{\rm h}_{\rm rvidlines}$) is 23 km s^{-1}. For comparison, Harris (1996) gives a mean heliocentric radial velocity of -22.8 ± 0.2 km s^{-1} for M71. As the sample spectra have a resolution $R \sim 2000$, we expect a theoretical accuracy of around $(1/10)(c/2000) = 15$ km s^{-1}, which is in good agreement with the scatter obtained above. Individually, the higher values in the measurements of the heliocentric radial velocities could be explained in part based on the low-resolution of the spectra. We found a nearly Gaussian distribution of the radial velocitites with a dispersion of ∼45 km s^{-1}, and we believe that this finding reflects the uncertainty in the determination of the radial velocity itself at this spectral resolution. The accuracy in the heliocentric radial velocities measurements is also wavelength-calibration dependent; in our case the GMOS calibration lamps were rather poor. Given the high velocity-dispersion obtained, the radial velocities were used to shift the sample spectra to rest wavelengths rather than a star membership selection criterion.

3.2. Photometry

As reported in the GEMINI/GMOS web site[1], up to September 12, 2006 there was a large (∼5″) offset in the optical positions (RA and Dec) in GMOS-North images. A FORTRAN code was applied in order to take these offsets into account and find out the correct identification of the sample stars from previous photometric catalogs of M71. Using the *SkyCat* tool we plotted all 145 observed stars on the Gemini-North preimaging and created our own finding chart of M71 following the identification as given in each GMOS mask. Optical photometry for M71 from the literature was adopted by selecting CCD photometry able to give us crucial information like completeness and membership probability. Two papers fulfilled these requirements: (i) Cudworth (1985) presents proper motions and visual photometry for 350 M71 stars down to a limit of $V = 16$. Cudworth (2006, priv. comm.) gives proper motions and photometry for fainter stars ($V > 16$), amounting to 1522 stars. (ii) Geffert & Maintz (2000) and Geffert (2002, priv. comm.) present B, V CCD observations for around 4450 stars (limited to $V = 18.5$ mag) covering a field of 20 × 20 arcmin of M71.

The colour–magnitude diagram (CMD) of M71, using the photometry from Cudworth (1985, 2006) and marking the sample stars is displayed in Fig. 1. Overplotted is a Yonsei-Yale isochrone (Kim et al. 2002) with parameters [Fe/H] = −0.68 dex,

[1] http://www.gemini.edu/sciops/instruments/gmos/gmosIndex.html

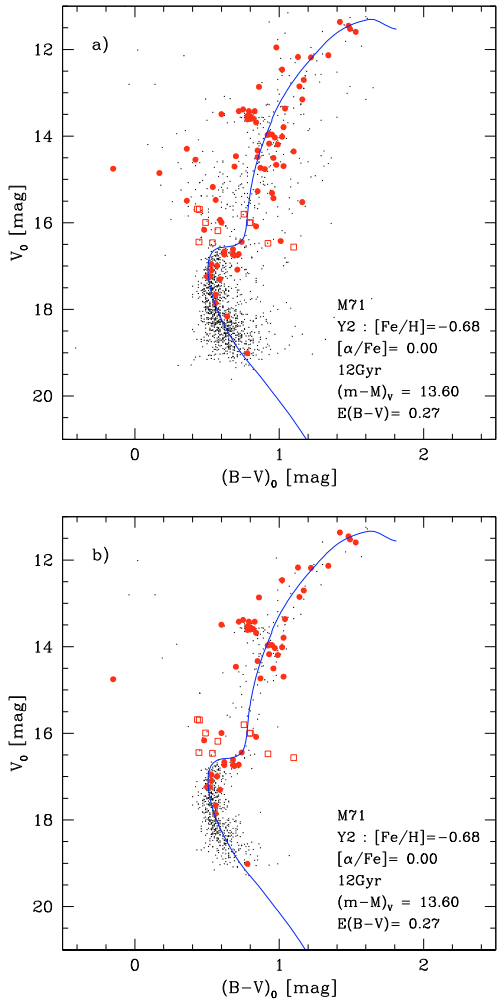

Fig. 1. The optical V, $B-V$ CMD of M71. *Top*: *dots*: Cudworth (1985, 2006) photometry; *filled circles*: sample stars; *open squares*: stars identified in Geffert & Maintz (2000). *Bottom*: stars with membership probability $P \geq 80\%$ (symbols are the same as above). A Yonsei-Yale isochrone by Kim et al. (2002) with parameters as indicated is overplotted.

[α/Fe] = 0.00 dex, age = 12 Gyr. The isochrone has been shifted by $(m-M)_V = 13.60$ mag and $E(B-V) = 0.27$ mag (Geffert & Maintz 2000). The stars' designations, positions, membership probabilities, colours, along with bolometric magnitudes, gravities and temperatures are shown in Table 1.

3.2.1. Temperatures

Effective temperatures ($T_{\rm eff}$) for the sample were obtained by employing the empirical calibrations of Alonso et al. (1996, 1999, 2001) for dwarfs and giants stars. The intrinsic colours $(B-V)_0$ were determined by adopting $E(B-V) = 0.27$ (Geffert & Maintz 2000) and mean [Fe/H] = −0.73 (Harris 1996). The uncertainty in the effective temperatures $T(B-V)$ derived using Alonso et al.'s calibrations is typically 150 K (within 1σ).

3.2.2. Surface gravities

Photometric gravities for all stars were obtained in the classical way, using the $T_{\rm eff}$s described in the previous section and adopting $M_* = 0.80\ M_\odot$, $(m-M)_V = 13.60$, $E(B-V) = 0.27$ (Geffert & Maintz 2000), with bolometric corrections taken from Alonso et al. (1999). Input solar values adopted were: $T_\odot = 5780$ K, $M_{\rm bol\odot} = 4.75$, and $\log g = 4.44$. The error in $M_{\rm bol}$ is mostly due to the M_V value and total extinction A_V, the latter with an uncertainty around ±0.05 mag. For M_V, adopting an error in distance as large as 30%, we get $\sigma_{M_{\rm bol}} \sim 0.30$ mag, which leads to an error on the adopted photometric gravities of ±0.30 dex. For stars fainter than $V = 17.5$, the surface gravities were derived from Yonsei-Yale 12 Gyr isochrones of $Z = 0.0040$, $Y = 0.24$ and [Fe/H] = −0.70 (Kim et al. 2002).

3.2.3. Spectral indices

The ability to analyze individual spectra of cluster members can provide knowledge on the spectral properties of stellar populations, placing constraints on stellar population synthesis. In medium-resolution spectra the measurement and analysis of spectral indices is widely employed to interpret the chemical evolution history of stellar populations in galaxies.

Absorption line indices were measured using the LECTOR program, by Vazdekis, which measures line strengths in 1D spectra (Vazdekis et al. 2003). Besides measuring the Lick/IDS absorption-line indices (Worthey et al. 1994; Worthey & Ottaviani 1997) we modified LECTOR in order to measure the line indices recently defined by Serven et al. (2005). In this paper, the only index from the latter list we will discuss is Al3953, which was shown by Serven et al. to be very sensitive to the abundance of aluminium.

For the uncertainties on the indices we initially considered those provided by LECTOR (see Cardiel et al. 1998, for details). These Poisson-based uncertainties on the indices are underestimated. Thus, the uncertainties were also estimated from the standard deviation of the measurements for each index on the individual spectra, and hereafter these latest uncertainties will preferentially be shown.

In Table 2 are presented the index passband definitions where wavelengths are given in angstroms. Tables 3−5 show the results and Poisson uncertainties in the total-passband net counts for the indices CN_1 [mag], CN_2 [mag], Ca4227 [Å], G4300:CH [mag], Fe4383 [Å], H_β [Å], Mg_1 [mag], Mg_2 [mag], Mgb [Å], Fe5270 [Å], Fe5335 [Å], Fe5406 [Å], NaD [Å] and Al3953 [Å], while Fig. 2 shows one of the final flux-calibrated spectra of the sample with some features labeled.

4. Results

The final sample adopted consists of stars with a membership probability higher than 80% and magnitudes $V \leq 15.5$ mag. In addition, each spectrum was individually inspected by the region of the index passbands. Below we present the main results.

4.1. CN and CH

The Lick CN indices measure the strength of the CN 4150 Å bandhead. Although we have measured CN_1 and CN_2, we chose to work with CN_1 more extensively. Both indices are similar in definition with a slight difference in their blue pseudocontinuum definition.

Figures 3a,b present the CN_1 index vs. V-band magnitude and $(B-V)_0$ colours for M71 selected stars. Stellar IDs are also marked. The distribution of the data points in these two plots is clearly bi-modal, with two families of stars with strong and weak CN bands at fixed colour and/or magnitude. The dividing line between CN-strong stars, it the top half, and CN-weak stars

Table 2. Index definition.

Index (1)	Blue Pseudocontinuum (2)	Feature (3)	Red Pseudocontinuum (4)
CN_1	4081.375 4118.875	4143.375 4178.375	4245.375 4285.375
CN_2	4085.125 4097.625	4143.375 4178.375	4245.375 4285.375
Ca4227	4212.250 4221.000	4223.500 4236.000	4242.250 4252.250
G4300	4267.625 4283.875	4282.625 4317.625	4320.125 4336.375
Fe4383	4360.375 4371.625	4370.375 4421.625	4444.125 4456.625
H_beta	4827.875 4847.875	4847.875 4876.625	4876.625 4891.625
Mg_1	4895.125 4957.625	5069.125 5134.125	5301.125 5366.125
Mg_2	4895.125 4957.625	5154.125 5196.625	5301.125 5366.125
Mgb	5142.625 5161.375	5160.125 5192.625	5191.375 5206.375
Fe5270	5233.150 5248.150	5245.650 5285.650	5285.650 5318.150
Fe5335	5304.625 5315.875	5312.125 5352.125	5353.375 5363.375
Fe5406	5376.250 5387.500	5387.500 5415.000	5415.000 5425.000
NaD	5862.375 5877.375	5878.625 5911.125	5923.875 5949.875
Al3953	3937.600 3967.400	3921.300 3935.500	3969.500 3987.000

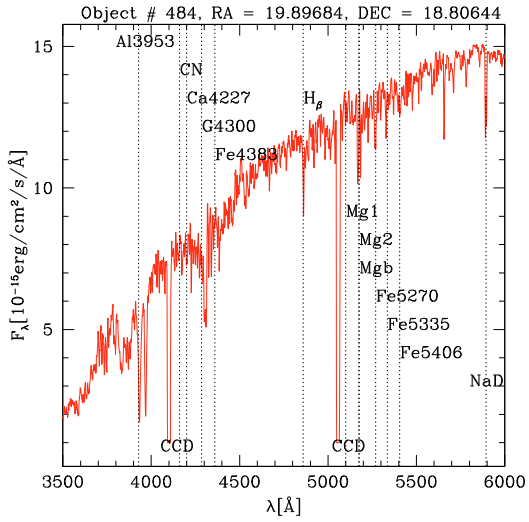

Fig. 2. Spectrum of the star 484 (1−55, V = 14.26) observed in the Mask # 2. Gaps are due to the 3 CCD configuration of the detector. Central wavelengths of studied indices are indicated.

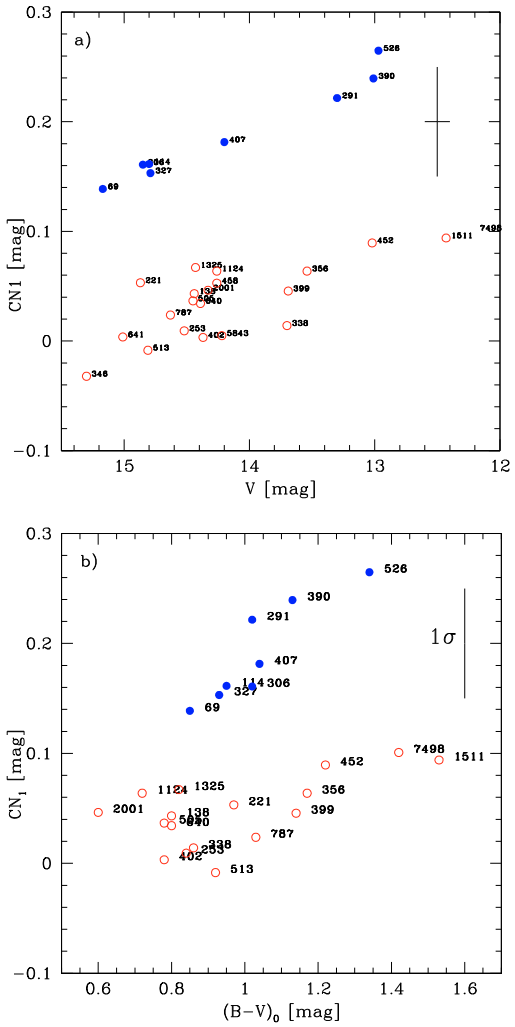

Fig. 3. a) CN_1 plotted against V, and **b)** CN_1 vs. $(B-V)_0$ for the M71 sample stars, where the locus CN-strong (*filled circles*) and CN-weak (*open circles*) are seen. Error bars quoted correspond to the rms on all measurements available.

in the bottom half of the plots runs diagonally from the lower left to the top right of both plots. This is because in both families of stars, CN is a strong function of temperature, so that CN-bands become stronger for lower temperatures in both the CN-strong and CN-weak groups. It is interesting that stars 291, 390 and 526 are AGB members, and they show a higher N enhancement.

Concerning stars 1351, 1556 and 640, their CN measurements were slightly affected by the presence of the 2 CCD gaps around their red passband. For the CN-strong stars, showing nitrogen excesses, we found $\langle CN \rangle = 0.19 \pm 0.04$ (N = 8 stars), whereas for the CN-weak stars $\langle CN \rangle = 0.04 \pm 0.04$ (N = 20 stars). Note that stars 1351, 1556 and 640 were not taken into consideration in computing the mean CN-weak value.

In Fig. 4 we show the location of CN-strong and CN-weak stars in the CMD, for $V < 15.5$. Stars weaker than $V > 15.5$ are also plotted, with no distinction between CN intensities, given the lower S/N of the spectra. In Fig. 5 the CN_1 index vs. $T_{\rm eff}$ is shown for the giants, where the bimodality of CN-strength is found among both RGB and Asymptotic Giant Branch (AGB) stars. Figure 6 shows CN_1 vs. log g for all stars, illustrating the clear separation between CN-strong and CN-weak giants, whereas for dwarfs, the bimodality is not so clear, partly due to the lower S/N of our dwarf-star spectra, and partly because the differences between CN-strong and CN-weak spectra are more subtle, given that CN-bands are weak overall in the spectra of warm turnoff stars. Recall however that Cohen (1999) has found a bimodality for main sequence (MS) stars of M71.

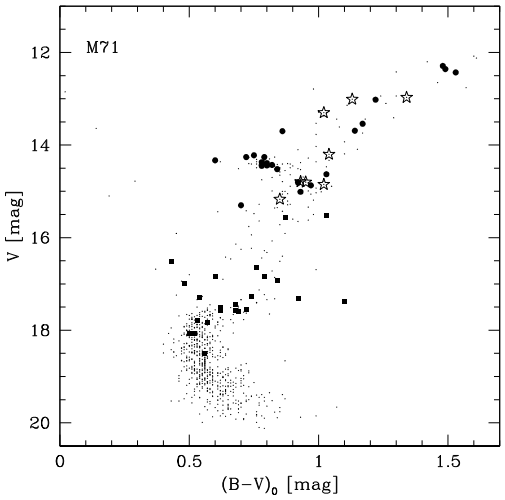

Fig. 4. V, $B-V$ CMD with the CN-strong stars (*open stars*), CN-weak (*filled circles*), and the subgiants (*filled squares*) for which the CN measurements are not qualified as strong or weak.

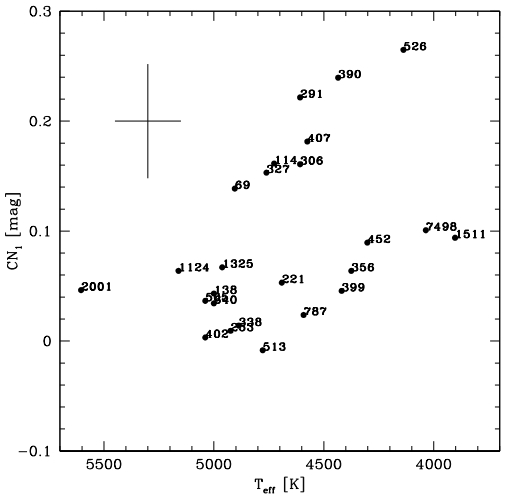

Fig. 5. CN_1 vs. effective temperature. Error bar on CN_1 is as explained in Fig. 3, while on $T_{\rm eff}$ it resembles the value determined with the photometric calibration employed.

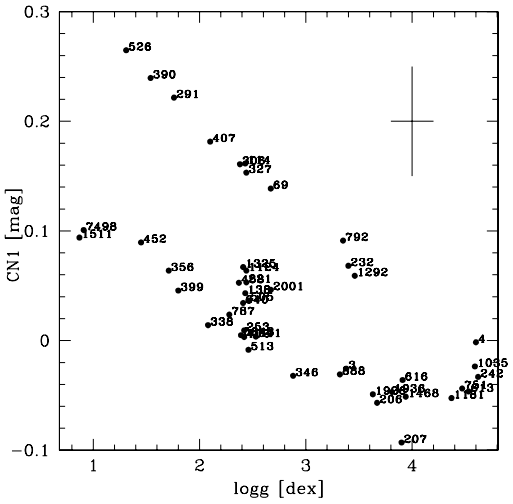

Fig. 6. CN_1 vs. log g. Error bar is indicated.

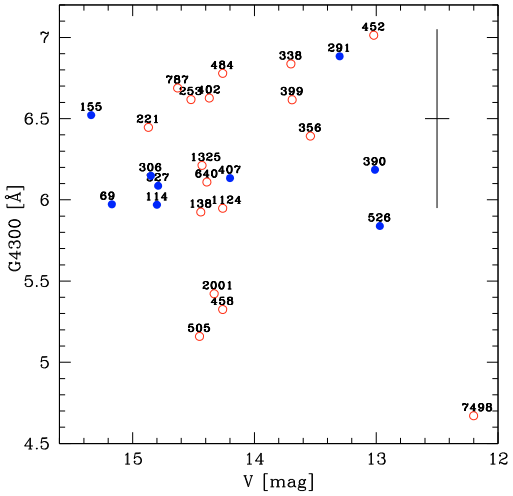

Fig. 7. G-band as function of V magnitude, where CN-strong (*filled circles*) and CN-weak (*open circles*) stars are plotted separately.

The G-band at 4300 Å includes a CH bandhead and can be used to derive the carbon abundance. Its behaviour along the main sequence, subgiant and red giant sequences can give important clues on mixing processes along stellar evolution. In Fig. 7 we plot the G band indices as a function of V magnitude. The symbols are the same as used in Figs. 3a,b, where the CN-strong and CN-weak sequences are represented by filled and open circles. One can see that CN-strong stars tend to present lower CH values, while the CN-weak stars appear to show higher values of CH. This general trend confirms the well-known CN-CH anticorrelation in giant stars reported in past decades for many Galactic globular clusters (e.g., Dickens et al. 1979; Smith 1987; Kraft 1994; Gratton et al. 2004, and references therein). Note, however, that despite their high membership probabilities, stars 2001, 458, 505 and 7498 present lower G-band strengths than other CN-weak stars of the sample. Stars 2001, 458 and 505 are HB members, and this suggests that we also detect a bimodal distribution in the HB. Figure 8 plots an example of CN-bimodality and CN-CH anticorrelation for two M71 stars of similar V magnitude and $T_{\rm eff}$. The CN-strong giant 390 (T = 4435 K : CN = 0.24 : CH = 6.18) presents a stronger CN band and a weaker CH band strength than star 399 (T = 4419 : CN = 0.04 : CH = 6.62).

4.2. Iron and magnesium indices

We measured spectral indices sensitive to the abundances of iron (Fe4383, Fe5270, Fe5335, and Fe5406) and magnesium (Mg_1, Mg_2 and Mgb) in all our spectra. We henceforth focus on an average Fe index, defined as $\langle$Fe$\rangle$ = (Fe4383 + Fe5270 + Fe5335 + Fe5406)/4 and Mg_2. All these indices are of widespread use in stellar population studies in galaxies and stellar clusters. Figure 9 plots the behaviour of Mg_2 as a function of CN and $T_{\rm eff}$, respectively. In this figure we see that both CN-weak and CN-strong sequences correspond to $Mg_2 \geq 0.05$ mag and Mg_2 tends to be higher for cooler stars ($T_{\rm eff} \leq 4300$ K). Therefore, Mg_2 is weaker in CN-strong stars, and this seems to indicate that besides a Mg-Al anticorrelation (Fig. 14), and a weak Al-CN anticorrelation (Fig. 13), we found some evidence for a Mg-N anticorrelation (see Gratton et al. 2004).

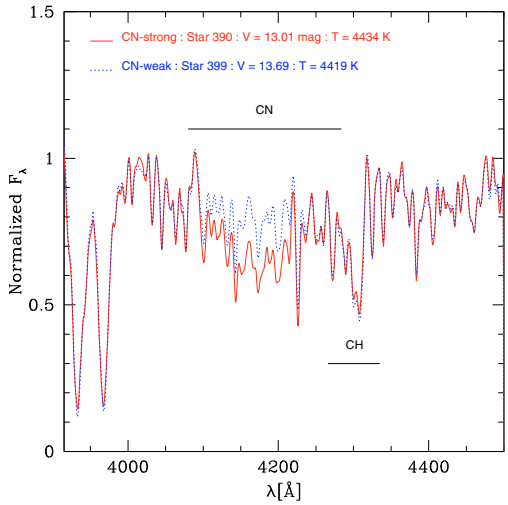

Fig. 8. Stars 390 and 399 in the molecular CN and CH band region. The full and dashed lines represent the CN-strong and CN-weak stars, respectively. These stars display approximately the same temperatures.

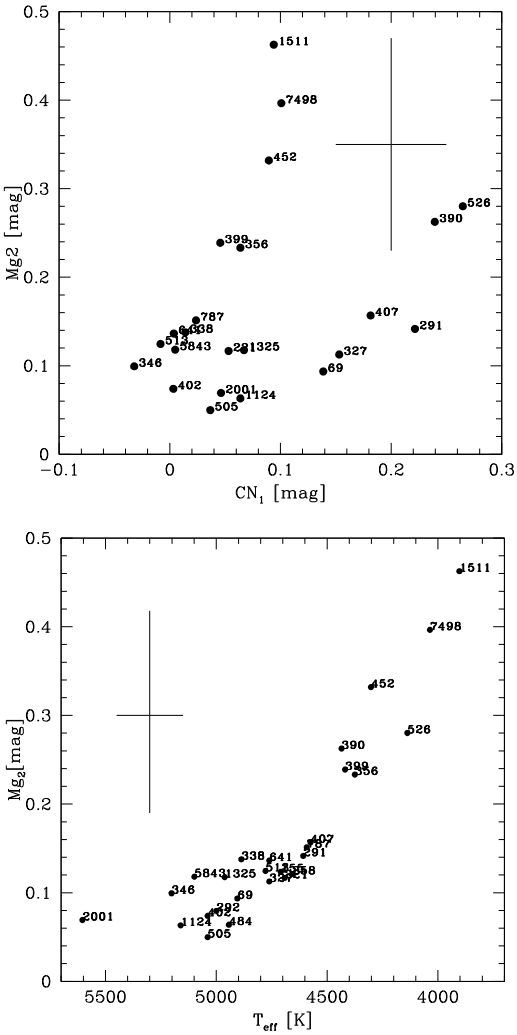

Fig. 9. *Upper panel*: Mg_2 plotted against CN_1; *lower panel*: Mg_2 as a function of the effective temperature. Error bars are as previously discussed.

4.3. Ca4227

This index is widely used in stellar population studies in galaxies, where Ca is considered as a representative α-element (e.g. Thomas et al. 2003; Prochaska et al. 2005). We found $\langle$Ca4227$\rangle$ = 1.25 ± 1.00 Å for 32 stars in the range $12 \leq V \leq 15.5$ and with a membership probability higher than 80%.

Figures 10 and 11 show the behaviour of Ca4227 as a function of $T_{\rm eff}$ and the metallicity indicators $\langle$Fe$\rangle$ and Mg_2 indices, respectively. By comparing Figs. 9 with 10, a similarity between the general behaviour of Ca4227 and Mg_2 indices with $T_{\rm eff}$ is seen. This explains the behaviour presented between Ca4227 and Mg_2 in Fig. 11. All these findings show that the cooler giants with higher metallicity indicators also show high Ca4227 indices. These figures also show that the metallicity indices Mg_2 and $\langle$Fe$\rangle$ grow non-linearly at low temperatures.

4.4. H_β

H_β index is widely used as an age indicator in stellar population studies and is known to be extremely temperature- and gravity-dependent. We found a mean H_β index of $\langle H_\beta \rangle$ = 1.57 ± 0.68 Å (N = 31). We notice that there is a large variation of H_β measurements for stars with $V < 14$ and this effect appears to be real since Figs. 12a,b suggest a higher dispersion on the H_β measurements for stars cooler than 4500 K.

4.5. NaD and Al3953

NaD and Al3953 features included in the present analysis are as defined in Worthey et al. (1994) and Serven et al. (2005), respectively. As shown in Table 2 of Serven et al. (2005), the new index Al3953 has a high spectral response to aluminum abundance variations. However, although both are very useful indices able to rule out important clues for understanding the abundance variations in stellar populations, they are composed of resonance lines and subject to effects from interstellar absorption, that have to be taken into account when trying to interpret them. We found $\langle$NaD$\rangle$ = 4.60 ± 2.38 Å (N = 28) and $\langle$Al3953$\rangle$ = 2.76 ± 1.35 Å (N = 25).

Figure 13 displays the behaviour of NaD and Al3953 as a function of the CN band, while Fig. 14 shows the behaviour of NaD and Mg_2 indices against the new index Al3953. An Na-Al anticorrelation is clearly seen.

4.6. Fitting functions

The fitting functions approach is a useful tool at low resolution to derive abundances that are both reddening and distance modulus independent. In this section, we use the fitting functions derived by Barbuy et al. (2003) for the indices Fe5270, Fe5335 and Mg_2, as a function of stellar parameters, in order to estimate metallicities for M71 stars, based on the Lick index measurements presented in the previous sections.

The Fe5270, Fe5335 and Mg_2 features are known to be suitable metallicity indicators due to their relatively weak dependence on gravity and temperature. A relation between these indices and [Fe/H] was derived by Barbuy et al. (2003) based on synthetic spectra for resolutions of 8.3 Å and 3.5 Å. We use their Value1 fitting function coefficients for Fe5270, Fe5335 and Mg_2 computed with $FWHM$ = 3.5 Å, valid for $-3 \leq$ [Fe/H] $\leq +0.3$, $0 \leq \log g \leq 3$ and $4000 \leq T_{\rm eff} \leq 7000$.

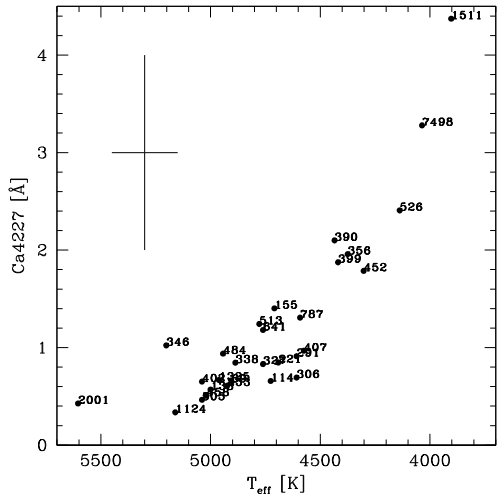

Fig. 10. Ca4227 feature against the effective temperature.

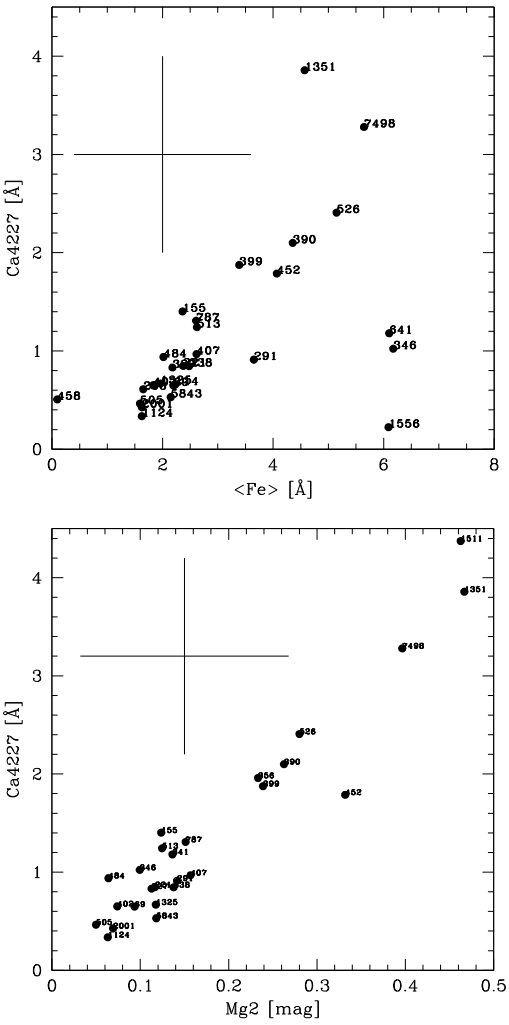

Fig. 11. *Upper panel*: Ca4227 vs. ⟨Fe⟩, and *lower panel*: Ca4227 vs. Mg_2. ⟨Fe⟩ = (Fe4383 + Fe5270 + Fe5335 + Fe5406)/4.

A mean Fe = (Fe5270+Fe5335)/2 and Mg_2 indices were used as metallicity indicators. Mean values of ⟨Fe5270⟩ = 2.70 ± 1.47 (N = 30), ⟨Fe5335⟩ = 2.53 ± 1.48 (N = 29) and ⟨Mg_2⟩ = 0.17227 ± 0.11828 (N = 28) were obtained for giants. Based on stars in the range 4500 < $T_{\rm eff}$ < 5000 K (validity of the fitting

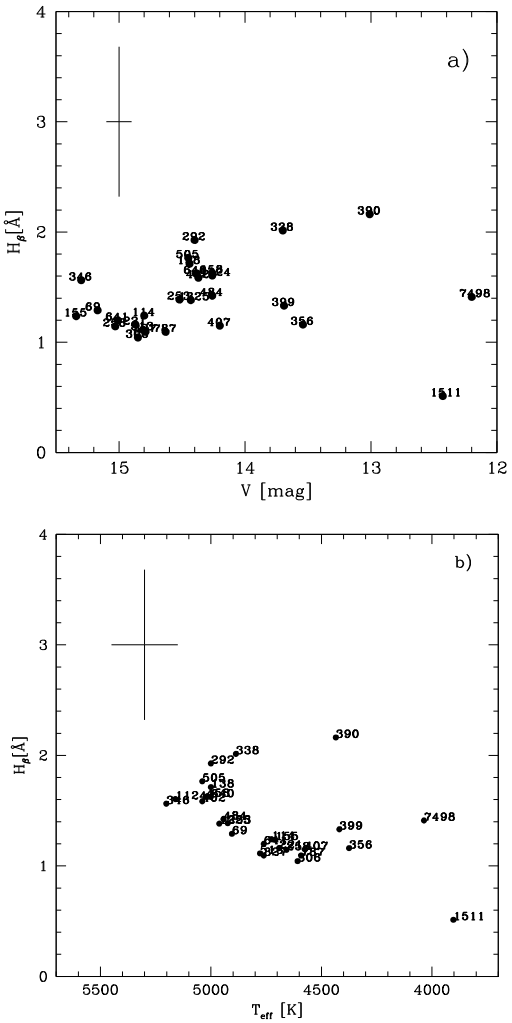

Fig. 12. a) H_β plotted against V, and **b)** H_β against $T_{\rm eff}$.

functions for Mg_2, mean values of Fe5270 = 2.21 ± 0.72 (18 giants), Fe5335 = 2.04 ± 0.63 (17 giants) and Mg_2 = 0.12 ± 0.03 (11 giants) are found.

Adopting mean parameters $T_{\rm eff}$ = 4768 K and log g = 2.29 dex, metallicities of [Fe/H] = −0.81, −0.91 and −0.68, corresponding to Fe5270, Fe5335 and Mg_2 respectively, are obtained. In Table 6 are reported [Fe/H] values from high-resolution spectroscopy and those from fitting functions, where a good agreement is found.

4.7. Spectrum synthesis

By adopting [Fe/H] ≈ −0.8 for M71, taking into account the values given in Table 6, we carried out a spectrum synthesis calculation of CN and CH bands in the wavelength region 4000−4400 Å. The code is described by Cayrel et al. (1991) and Barbuy et al. (2003), where CN and CH line lists are from Kurucz (1993), and implemented in our code as described in Castilho et al. (1999). MARCS model atmospheres from Gustafsson et al. (2006) were used.

Synthetic spectra were computed for a pair of CN-weak/CN-strong stars with similar stellar parameters: stars 390 and 399, with ($T_{\rm eff}$, log g, $v_{\rm t}$) = (4434 K, 1.54, 1.5 km s^{-1}) and (4419 K, 1.8, 1.5 km s^{-1}). Carbon and nitrogen abundances were found to be of [C/Fe] = 0.0, [N/Fe] = +1.0 for the CN-strong

Table 6. Literature and present values of metallicity for M71.

[Fe/H]	[FeI/H]	[FeII/H]	Method	Reference
−0.79	−0.79	−0.79	High-resolution: 10 giants	Sneden et al. (1994)
−0.73	—	—	Compilation	Harris (1996)
−0.71	−0.71	−0.84	High-resolution: 25 stars	Ramirez et al. (2001)
−0.82	−0.81	−0.82	Revision of Sneden et al.'s 10 giants	Kraft & Ivans (2003)
−0.80	−0.81	−0.85	High-resolution: 5 dwarfs	Boesgaard et al. (2005)
−0.81	—	—	Fitting Functions	Fe5270 index (Present work)
−0.91	—	—	Idem	Fe5335 index (Present work)
−0.68	—	—	Idem	Mg_2 index (Present work)

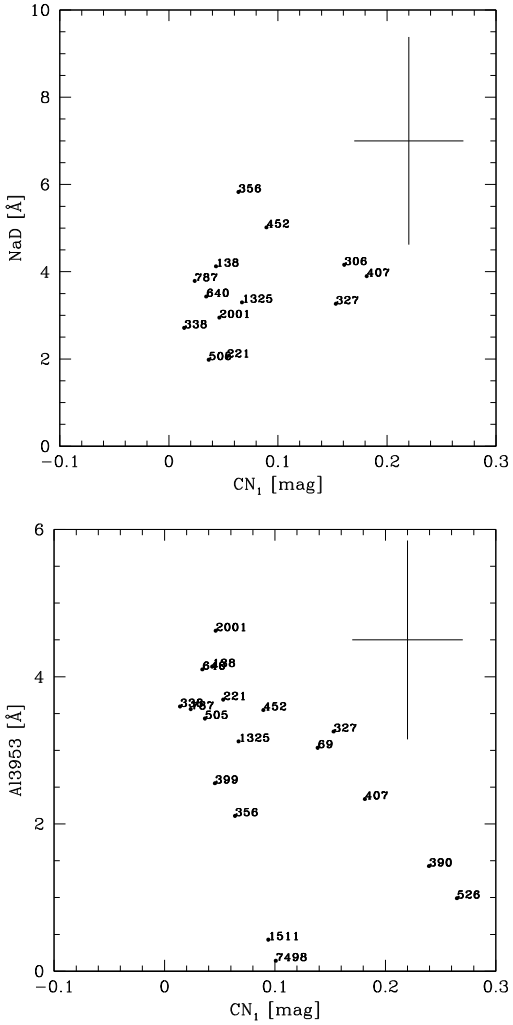

Fig. 13. NaD and Al3953 as a function of the CN index.

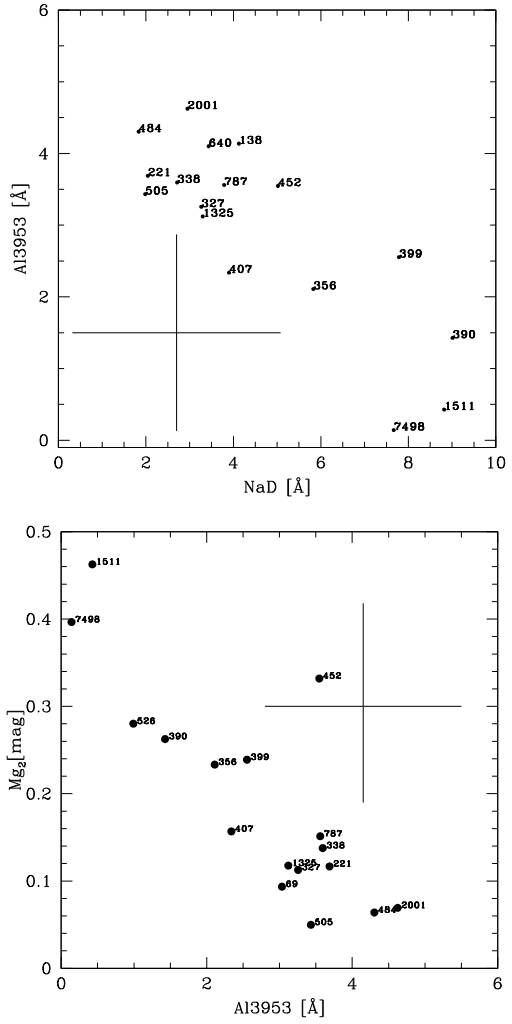

Fig. 14. *Top*: Al3953 vs. NaD. *Bottom*: Mg_2 vs. Al3953.

star 390 and [C/Fe] = 0.0, [N/Fe] = +0.50 for the CN-weak star 399, assuming [O/Fe] = +0.3 in both cases. The difference in nitrogen abundances is clear, as shown in Fig. 15.

5. Discussion

The light elements C, N, O, Na, Mg and Al show variations in globular cluster stars. In M71 a bimodal distribution of CN-strong and CN-weak stars and an anticorrelation between CN and CH were first made evident by Smith & Norris (1982). For stars brighter than the Horizontal Branch (HB) level they showed that CN and CO are anticorrelated, and CN correlated with Na. Smith & Penny (1989) measured CN and CH based on the bandheads CN 3883 Å, CN 4215 Å and CH 4300 Å for a sample of HB stars in M71, and revealed an anticorrelation between CN and CH. CN-strong and CN-weak components were also revealed by Penny et al. (1992), who also showed an anticorrelation CN-CH for subgiants in M71. A CN-bimodality and a CN-CH anticorrelation were also found for a sample of 79 MS stars in M71 by Cohen (1999). Briley et al. (2001) further derived CN and CH for 75 giants of M71 based on DDO photometric indices C(41−42) and C(42−45), and confirmed the C vs. N anticorrelation and the CN-strong and CN-weak components. Lee (2005) studied CN and CH band strength variations in 14 M71 giants showing clearly the CN bimodality, whereas the CN-CH anticorrelation is not clear in his analysis.

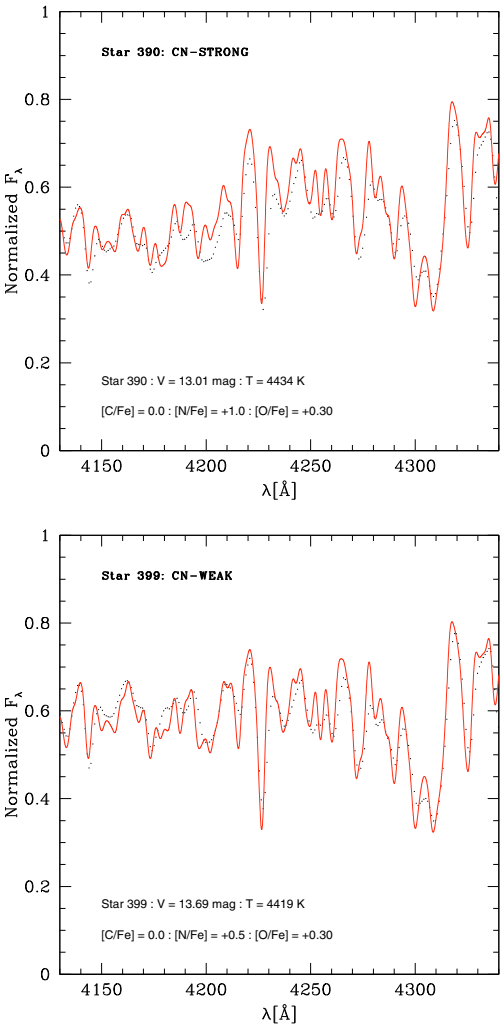

Fig. 15. Synthetic (solid line) and observed spectra (dotted line) in the region of CN and CH bands. *Upper panel*: star 390 (CN-strong): $T_{\rm eff}$, log g, $v_{\rm t}$) = (4434 K, 1.54, 1.5 km s^{-1}) computed for [C/Fe] = 0.0, [N/Fe] = +1.0; *lower panel*: star 399 (CN-weak): (4419 K, 1.8, 1.5 km s^{-1}) computed for [C/Fe] = 0.0, [N/Fe] = +0.50.

The behaviour of the CN and CH bands above is also reported for stars on the RGB and MS of 47 Tuc (see e.g. Norris & Freeman 1979; Norris et al. 1984; Cannon et al. 1998), another well studied Galactic globular cluster with metallicity close to that of M71 ([Fe/H] = −0.67, Alves-Brito et al. 2005). However, 47 Tuc is more massive than M71, as well as more concentraded with a half-mass radius $r_{\rm h}$ = 2.79 arcmin and concentration parameter c = 2.03, whereas M71 has $r_{\rm h}$ = 1.65 arcmin and c = 1.15 (Harris 1996).

Based on the Cudworth (1985; 2006) star designations, it was possible to identify several stars in common with other spectroscopic studies (e.g. in Smith & Penny 1989; Penny et al. 1992; Lee 2005), which allows us to do a direct CN-CH band-strength comparison. The cross-check is possible for 15 out of 22 stars overlapping with our sample – 4 stars have no CN measurements in the literature, whereas we have no CN measurements for 3 other stars due to the position of the CCD gaps in their spectra. The comparison shows that 13 out of 15 stars present the same classification of CN-weak or CN-strong found in the present work, while 2 stars were found to present a different classification – stars 1−43 and 1−88 were previously classified as CN-strong. On the other hand, within a 1σ-uncertainty, those authors present the same CN values.

Regarding our CN-CH strength results, Fig. 7 illustrates the CN bimodality and CN-CH anticorrelations. Note, however, as discussed above, that 3 stars (IDs 1556, 1351 and 640) have inaccurate CN measurements due to the CCD gaps. Stars 2001, 458, and 505, which are classified as CN-weak, show lower CH values than other CN-weak stars. Even with some statistical outliers our CN-CH distribution has similar proportions as those given in Smith & Norris (1982).

Within the canonical framework of stellar structure and evolution of low-mass stars, the enhancement of nitrogen followed by the depletion of carbon in the CN-strong stars is attributed to the dredge-up of CN-processed material into the surface layers of such stars (Iben 1964; Charbonnel 1994). The present CN variations followed by an anticorrelation in the CH band confirm that an episode of deep mixing occurred in the M71 giants studied. On the other hand, the CN bimodality is better explained within a primordial pollution scenario. The mixing hypothesis does not explain the behaviour seen for the positive correlation between CN-Na and CN-Al, given that Na and Al are not produced during these mixing events.

Elements such as Al and Mg are produced by p-capture at higher temperatures (e.g. Langer & Hoffman 1995). As shown in Fig. 14, there is a clear anticorrelation between Al3953 vs. NaD and Mg_2 indices. The Al-Mg anticorrelation seen in some globular cluster red giants is well explained by the enhanced extra mixing discussed in Denissenkov & VandenBerg (2003). Ramirez & Cohen (2002) reported a [Na/Fe]:[Al/Fe] correlation for their sample of M71 stars, however their results show a 2σ uncertainty (see their Fig. 13).

A scenario that appears plausible is that CNO-processed material in intermediate mass stars (IMS) on the AGB occurs early in the cluster's life, and their stellar winds are captured by low-mass stars (Gratton et al. 2004) or else by fast rotating massive stars (Decressin et al. 2007). Both the AGB or massive star early pollution possibilities are consistent with scenarios of self-enrichment proposed by Cayrel (1986), Parmentier et al. (1999), Parmentier & Gilmore (2001), Thoul et al. (2002), and Bekki et al. (2007). The latter developed a model of globular cluster formation in the central regions of low mass proto-galaxies embedded in dark matter halos. These proto-galaxies would retain the AGB ejecta and cause an "external pollution" of the globular cluster stars. This model can explain the C-N and Mg-Al anticorrelations, but shows a strong disagreement with the observed O-Na anticorrelation.

For the present sample, we found that CN and Na are correlated, while a CN-Al correlation does not appear. These CN-Na results imply a primordial explanation for abundance variations in M71.

6. Summary and conclusions

In M71 previous studies such that of Smith & Norris (1982) that first showed a bimodal distribution of CN-strong and CN-weak stars and an anticorrelation between CN and CH. This was followed by Smith & Penny (1989), Penny et al. (1992), Briley et al. (2001), Cohen (1999), Ramirez et al. (2001), Ramírez & Cohen (2002), Boesgaard et al. (2005), and Lee (2005).

We measured CN, CH, Ca4277, iron and magnesium indicators, H$_\beta$, NaD and Al3953 spectral indice, from low-resolution spectra of 89 stars of the metal-rich globular cluster M71, observed with the Gemini Multi-Object Spectrograph (GMOS) at

the Gemini-North telescope. CN and CH strengths were obtained for 89 stars, among which 33 giants. As expected from evolutionary mixing theories and additional extra-mixing (Iben 1964; Charbonnel 1994; Denissenkov & VandenBerg 2003), we find a CN-CH anticorrelation. We find CN-strong and CN-weak stars, with around 30% of CN-strong ones, similar to other clusters such as NGC 6752 with about 50%.

We confirm a CN-bimodality besides the CN-CH anticorrelation, a CN-Na correlation, and Al-Na and Mg_2-Al anticorrelation. The interpretation of CN bimodality is instead better understood in terms of primordial variations, and possible scenarios include an early enrichment by winds from intermediate mass stars in the AGB phase, and captured by low-mass stars, early in the cluster's life (Gratton et al. 2004, and references therein; Bekki et al. 2007) or early pollution by fast rotating massive stars (Decressin et al. 2007).

CN-strong and CN-weak bimodality is only seen in relatively metal-rich globular clusters, but not in all of them. Such behaviour is well studied in particular in 47 Tucanae, NGC 6752 and M4. Such abundance variations in metal-rich globular clusters is undoubtedly one of the most intrincate challenges for the current theory of stellar evolution, and further observations with larger samples would be interesting.

Acknowledgements. A.A. acknowledges a FAPESP fellowship No. 04/00287-9. A.A. would like to thank the hospitality of the Department of Astronomy at the University of Virginia, during a visit in which part of this work was developed. Likewise, RPS would like to warmly thank the hospitality of the Astronomy Department at the University of São Paulo, during which much of this work was conceived. We are grateful to Professor Kyle Cudworth for cordially making his preliminary reduction of proper motions and photometry for M71 stars available to us. All observations were part of GEMINI Program GN-2002B-Q-42. This work is based on observations obtained at the Gemini Observatory, which is operated by the AURA, Inc., under a cooperative agreement with the NSF on behalf of the Gemini partnership: the NSF (United States), the PPARC (United Kingdom), the NRC (Canada), CONICYT (Chile), the ARC (Australia), CNPq (Brazil) and CONICET (Argentina).

References

Alonso, A., Arribas, S., & Martínez-Roger, C. 1996, A&AS, 313, 873
Alonso, A., Arribas, S., & Martínez-Roger, C. 1999, A&AS, 140, 261
Alonso, A., Arribas, S., & Martínez-Roger, C. 2001, A&A, 376, 1039
Alves-Brito, A., Barbuy, B., Ortolani, S., et al. 2005, A&A, 435, 657
Barbuy, B., Perrin, M.-N., Katz, D., et al. 2003, A&A, 404, 661
Bekki, K., Campbell, S. W., Lattanzio, J. C., & Norris, J. E. 2007, MNRAS, 377, 335
Boesgaard, A. M., King, J. R., Cody, A. M., Stephens, A., & Deliyannis, C. P. 2005, ApJ, 629, 832
Briley, M. M., Smith, G. H., & Claver, C. F. 2001, AJ, 122, 2561
Cannon, R. D., Croke, B. F. W., Bell, R. A., Hesser, J. E., & Stathakis, R. A. 1998, MNRAS, 298, 601
Cardiel, N., Gorgas, J., Cenarro, J., & Gonzalez, J. J. 1998, A&AS, 127, 597
Castilho, B., Spite, F., Barbuy, B., et al. 1999, A&A, 345, 249
Cayrel, R. 1986, A&A, 168, 81
Cayrel, R., Perrin, M.-N., Buser, R., Barbuy, B., & Coupry, M.-F. 1991, A&A, 247, 122
Charbonnel, C. 1994, A&A, 282, 811
Coelho, P., Barbuy, B., Meléndez, J., Schiavon, R., & Castilho, B. 2005, A&A, 443, 735
Cohen, J. 1999, AJ, 117, 2434
Cohen, J. G. 1980, ApJ, 241, 981
Cohen, J. G., Gratton, R. G., Behr, B. B., & Carretta, E. 1999, ApJ, 523, 739
Cudworth, K. M. 1985, AJ, 90, 65
Decressin, T., Meynet, G., Charbonnel, C., Prantzos, N., & Ekström, S. 2007, A&A, 464, 1029
Denissenkov, P. A., & VandenBerg, D. A. 2003, ApJ, 593, 509
Dickens, R. J., Bell, R. A., & Gustafsson, B. 1979, ApJ, 232, 428
Dinescu, D. I., Girard, T. M., & van Altena, W. F. 1999, AJ, 117, 1792
Geffert, M., & Maintz, G. 2000, A&AS, 144, 227
Gratton, R., Sneden, C., & Carretta, E. 2004, ARA&A, 42, 385
Grundahl, F., Stetson, P. B., & Andersen, M. I. 2002, A&A, 395, 481
Gustafsson, B., Edvardsson, B., Eriksson, K., et al. 2008, A&A, 486, 951
Harris, W. E. 1996, ApJ, 112, 1487
Hesser, J. E., Hartwick, F. D. A., & McClure, R. D. 1977, ApJS, 33, 471
Hook, I. M., Jorgensen, I., Allington-Smith, J. R., et al. 2004, PASP, 116, 425
Iben, I. Jr. 1964, ApJ, 140, 1631
Kim, Y.-C., Demarque, P., Yi, S. K., & Alexander, D. 2002, ApJS, 143, 499
Kurúcz, R. L. 1993, CD-ROM, 23
Lee, S.-G. 2005, JKAS, 38, 23
Lee, Jae-Woo, Carney, B. W., & Balachandran, S. C. 2004, AJ, 128, 2388
Kraft, R. P. 1994, PASP, 106, 553
Kraft, R. P., & Ivans, I. I. 2003, PASP, 115, 143
Langer, G. E., & Hoffman, R. D. 1995, PASP, 107, 1177
Leep, E. M., Wallerstein, G., & Oke, J. B. 1987, AJ, 93, 338
Meissner, F., & Weiss, A. 2006, A&A, 456, 1085
Norris, J., & Freeman, K. C. 1979, ApJ, 230, L179
Norris, J., Freeman, K. C., & Da Costa, G. S. 1984, ApJ, 277, 615
Parmentier, G., & Gilmore, G. 2001, A&A, 378, 97
Parmentier, G., Jehin, E., Magain, P., et al. 1999, A&A, 352, 138
Penny, A. J., Smith, G. H., & Churchill, C. W. 1992, MNRAS, 257, 89
Prochaska, L. C., Rose, J. A., & Schiavon, R. P. 2005, AJ, 130, 2666
Ramírez, S., & Cohen, J. G. 2002, AJ, 123, 3277
Ramírez, S., Cohen, J. G., Buss, J., & Briley, M. M. 2001, AJ, 122, 1429
Serven, J., Worthey, G., & Briley, M. M. 2005, ApJ, 627, 754
Smith, G. H. 1987, PASP, 99, 67
Smith, G. H., & Norris, J. 1982, ApJ, 254, 149
Smith, G. H., & Penny, A. J. 1989, AJ, 97, 1397
Sneden, C., Kraft, R. P., Langer, G. E., Prosser, C. F., & Shetrone, M. D. 1994, AJ, 107, 1773
Thoul, A., Jorissen, A., Goriely, S., et al. 2002, A&A, 383, 491
Thomas, D., Maraston, C., & Bender, R. 2003, MNRAS, 343, 279
Vazdekis, A., Cenarro, A. J., Gorgas, J., Cardiel, N., & Peletier, R. F. 2003, MNRAS, 340, 1317
Worthey, G., & Ottaviani, D. L. 1997, ApJS, 111, 377
Worthey, G., Faber, S. M., Gonzalez, J., & Burstein, D. 1994, ApJS, 94, 687
Yong, D., Aoki, W., & Lambert, D. L. 2006, ApJ, 638, 1018